

24
25
26
27
28
29
30
31
32
33
34
35
36
37
38
39
40
41
42
43
44
45
46

Abstract

This study shows that the four main phases of springtime El Niño-Southern Oscillation (ENSO) evolution (persistent versus early-terminating El Niño, and resurgent versus transitioning La Niña) are linked to distinctive spatial patterns of the probability of U.S. regional tornado outbreaks. In particular, the outbreak probability increases significantly up to 27% over the Ohio Valley, Upper Midwest and Southeast when a La Niña persists into the spring and is followed by another La Niña (i.e., resurgent La Niña). The probability also increases significantly up to 38%, but mainly in the South, when a two-year La Niña transitions to an El Niño (i.e., transitioning La Niña). This study also shows that the North Atlantic sea surface temperature tripole is linked to the tornado outbreak probability over the Southeast and Upper Midwest in early spring, although this link may not be completely distinct from ENSO. These changes in outbreak probability are shown to be largely consistent with remotely forced regional changes in the large-scale tropospheric circulation, low-level wind shear, moisture transports and extratropical storm activity.

47 **1. Introduction**

48 The latest U.S. Natural Hazard Statistics reported that during 2004-2013 tornadoes claimed
49 1,091 lives in the U.S., only trailing behind heat-related fatalities, and caused 21.6 billion dollars
50 in property and crop damages (Table S1). An early prognosis of tornadogenesis combined with
51 an effective warning system will prevent many deaths and serious injuries. A parallel effort to
52 expand the current severe weather outlooks beyond seven days will also help emergency
53 managers, government officials, businesses and the public to better prepare their resources to
54 save lives and to protect critical infrastructure.

55 As summarized in a recent review [Tippet *et al.*, 2014], notable advances have been made
56 since 2011, the year of the record-breaking tornado outbreaks in the U.S., on the potential of
57 expanding the severe weather outlook at the National Oceanic and Atmospheric Administration
58 (NOAA) beyond weather time scales [Tippett *et al.*, 2012; Weaver *et al.*, 2012; Barrett and
59 Gensini, 2013; Lee *et al.*, 2013; Thompson and Roundy, 2013; Elsner and Widen, 2014; Allan *et*
60 *al.*, 2015]. Among others, Lee *et al.* [2013] showed that the majority of the extreme U.S. tornado
61 outbreaks in the most intense tornado months of April and May during 1950-2010 were linked to
62 a positive Trans-Niño (i.e., a positive zonal gradient of sea surface temperature anomalies
63 (SSTAs) from the central tropical Pacific (CP) to the eastern tropical Pacific (EP)), typically
64 occurring during the boreal spring following the peak of La Niña [Trenberth and Stepaniak,
65 2001; Lee *et al.*, 2014a]. They showed using observations and modeling experiments that a
66 positive Trans-Niño could enhance large-scale atmosphere conditions conducive to intense
67 tornado outbreaks over the U.S. via extratropical teleconnections. Recently, Allen *et al.* [2015]
68 showed that La Niña events persisting into the spring could increase U.S. tornado activity,
69 especially over Oklahoma, Arkansas and northern Texas, and vice versa for El Niño events

70 persisting into the spring. They used March-April-May (MAM) SSTAs in the Nino3.4 region
71 (120°W-180°W and 5°S-5°N) to identify El Niño-Southern Oscillation (ENSO) events persisting
72 into the spring. *Krishnamurthy et al.* [2015] further showed that the seasonal phasing of ENSO is
73 critical to its impacts on the North American low-level jets, which influence U.S. tornado
74 activity by controlling low-level vertical wind shear and moisture availability [*Muñoz and*
75 *Enfield*, 2011; *Weaver et al.*, 2012].

76 These recent findings have identified ENSO as a potential source of seasonal predictability
77 for U.S. tornado activity. However, it should be noted that ENSO usually decays rapidly in
78 spring, which is the most active tornado season, shortly after reaching its peak in winter. During
79 this time, the SSTAs in the tropical Pacific are typically much weaker in amplitude and their
80 spatial structure becomes much less coherent [e.g., *Lee et al.* 2014a]. Additionally, every ENSO
81 event is somewhat different from others, which is especially true during the springtime ENSO
82 phase evolution [*Trenberth and Stepaniack*, 2001; *Chiang and Vimont*, 2004; *Yu and Kim*, 2010;
83 *Lee et al.*, 2014a; *Yeh et al.*, 2014; *Capotondi et al.*, 2015]. For example, an ENSO event, while
84 weakening during or after spring, may subsequently evolve into the onset of another ENSO event
85 with either the same or opposite sign in the subsequent months (e.g., 1986-1987 El Niño, 1987-
86 1988 El Niño and 1988-1989 La Niña). Hence, it is unlikely that the complexity of springtime
87 ENSO phase evolution can be characterized by using a single ENSO index such as the Nino3.4
88 index or Trans-Niño index.

89 Given the previous finding that ENSO may provide the seasonal predictability of U.S.
90 tornado outbreaks in spring, there is a clear need to better characterize the springtime ENSO
91 phase evolution and its link to U.S. tornado activity. On this issue, a new method was recently
92 presented to objectively characterize and explore the differences in the space-time evolution of

93 equatorial Pacific SSTAs observed during El Niño events [*Lee et al.*, 2014b]. An application of
94 this method to the 21 El Niño events during 1949-2013 captured two leading orthogonal modes,
95 which explain more than 60% of the inter-event variance. The first mode distinguishes a strong
96 and persistent El Niño from a weak and early-terminating El Niño (Figures 1a and 1b). A similar
97 analysis applied to the 22 La Niña events during 1949-2013 also revealed two leading orthogonal
98 modes, with its first mode distinguishing a resurgent La Niña and a transitioning La Niña
99 (Figures 1c and 1d).

100 The main objective of this study is to further advance our understanding of the relationship
101 between the springtime ENSO phase evolution and regional U.S. tornado outbreaks. To achieve
102 this and to move forward with the goal of developing a seasonal outlook for U.S. tornado
103 outbreaks, we first present a new metric to measure the probability of tornado outbreaks within
104 an area centered at a given geographic location (section 2). Then, we use that metric to explore
105 the probability of tornado outbreaks in various regions of the U.S. under the four dominant
106 phases of springtime ENSO evolution identified in *Lee et al.* [2014b] (section 3) and to explain
107 the associated atmospheric processes (section 4). We also report a potential link between the
108 North Atlantic SST tripole and U.S. regional tornado outbreaks in early spring (section 5).
109 Finally, we discuss further research that is needed to develop a seasonal outlook (section 6).

110

111 **2. Statistical Methods and Data Used**

112 To develop a seasonal outlook for U.S. tornado outbreaks, it is important to understand
113 exactly what a seasonal outlook can and cannot predict. First of all, tornadogenesis is a
114 mesoscale problem that requires overlap of very specific and highly localized atmospheric
115 conditions [e.g., *Doswell and Bosart*, 2001]. Therefore, it cannot be adequately captured by

116 large-scale and long-term averaged atmospheric fields. In other words, a seasonal outlook cannot
117 pinpoint exactly when, where and how many tornadoes may strike. Instead, a seasonal outlook
118 may predict in terms of probability which regions are more vulnerable to, or more likely to
119 experience, a widespread outbreak of tornadoes.

120 To move forward with the goal of developing a seasonal outlook, we propose a tornado
121 outbreak index, which can be used to measure the probability that a tornado outbreak may occur
122 in a predefined region. The following steps describe a method to compute the proposed tornado
123 outbreak index for 1950 - 2014 using the Severe Weather Database (SWD) from NOAA. The
124 Fujita scale-0 (F0) tornadoes are excluded in our analysis to avoid a spurious long-term trend in
125 the SWD [e.g., *Verbout et al.*, 2006; *Lee et al.*, 2013]. Additionally, the number of F1-F5
126 tornadoes is weighted in such a way that one F_n tornado is treated as n number of F1 tornadoes.

127 1) The first step is to count the weighted number of F1-F5 tornadoes within a circle of 200 km
128 radius from the center of each $1^\circ \times 1^\circ$ grid point for 5 consecutive days. This is referred to as a
129 5-day overlapping tornado density - one value for each day and grid point.

130 2) The second step is to define the outbreak threshold as the 99th percentile of the tornado
131 density values for each calendar month and grid point. Note that different threshold values
132 are used for each grid point and calendar month to account for the regionally and seasonally
133 inhomogeneous distribution of tornado statistics.

134 3) The final step is to identify months with one or more *outbreak days* to construct the monthly
135 U.S. regional tornado outbreak index for each grid point.

136 For a subset of data, the numbers of outbreak and non-outbreak years can be counted to
137 compute the probability of U.S. regional tornado outbreaks. Figure S1 shows the outbreak
138 threshold values of the tornado density, and the 90th and 95th percentile probabilities of U.S.

139 regional tornado outbreaks for March, April and May, obtained by using the steps described
140 above.

141 In the following sections, we explore the probability of tornado outbreaks in various regions
142 of the U.S. under the four dominant phases of springtime ENSO evolution (Figure 1). We use the
143 Extended Reconstructed Sea Surface Temperature version 3b (ERSST3), an in situ analysis of
144 global monthly SST on a $2^\circ \times 2^\circ$ grid [Smith *et al.*, 2008], to compute the leading modes of ENSO
145 variability for the period of 1949-2013 as discussed in Lee *et al.* [2014b]. The Twentieth Century
146 Reanalysis (20CR) [Compo *et al.*, 2011] and the National Centers for Environmental Prediction-
147 National Center for Atmospheric Research (NCEP-NCAR) reanalysis [Kalnay *et al.*, 1996] are
148 also used to derive atmospheric anomalies associated with the four dominant phases of
149 springtime ENSO evolution.

150

151 **3. Springtime ENSO Phases and Their Links to U.S. Regional Tornado Outbreaks**

152 Figure 1 shows the time-longitude plots of the tropical Pacific SSTAs, averaged between 5°S
153 and 5°N , for the four leading cases of ENSO variability reproduced from Lee *et al.* [2014b]. The
154 first case exhibits strong and positive SSTAs in the EP during the peak season persisting
155 throughout the boreal spring (+1), and thus is referred to as a strong and persistent El Niño case
156 (e.g., 1982-1983 El Niño); hereafter, any month/season in an ENSO onset year is identified by
157 the suffix (0), whereas any month/season in an ENSO decay year by the suffix (+1). The second
158 case is characterized by relatively weak positive SSTAs in the CP during the peak season and a
159 rapid development of cold SSTAs in the EP shortly after the peak season, and thus is referred to
160 as a weak and early-terminating El Niño case (e.g., 1963-1964 El Niño). The third case describes
161 a La Niña persisting into the spring (+1) and evolving to another La Niña, and thus is referred to

162 as a resurgent La Niña case (e.g., 1998-1999 La Niña). This case is also frequently referred to as
163 a two-year La Niña in the literature [e.g., *DiNezio and Deser*, 2014]. Finally, the fourth case
164 describes a two-year La Niña transitioning to an El Niño, and thus is referred to as a transitioning
165 La Niña case (e.g., 1971-1972 La Niña). Note that these four leading cases of ENSO variability
166 mainly describe ENSO phase evolution in the spring (+1) following the peak of ENSO in boreal
167 winter. For more details on the atmosphere-ocean dynamics linked to the leading modes of
168 ENSO variability, the reader is referred to *Lee et al.* [2014b].

169 Figure 2 shows the composite SSTAs for the four dominant phases of springtime ENSO
170 evolution in MAM (+1) and the corresponding probability of regional tornado outbreaks in April
171 (+1). See Figures S3-S6 in the supporting information for the composite SSTAs and the
172 probability of outbreaks in March (+1) and May (+1). The gray dots indicate that the SSTAs are
173 statistically significant at 90% based on a Student's *t*-test. Similarly, the black dots mean that the
174 probability of tornado outbreaks is statistically significant at 90% based on the exact binomial
175 test of the null hypothesis, i.e., the springtime ENSO phases have no effect on the probability of
176 tornado outbreaks. For each case, we used eight to eleven actual ENSO events for the composite
177 analysis based on the sign and amplitude of the leading principal components of El Niño and La
178 Niña variability (see Table S2 for the list of ENSO events used).

179 As shown in Figures 2a and 2e, the probability of U.S. regional tornado outbreaks in April
180 (+1) is low overall (5% or less) when a strong El Niño persists into the spring (+1) after its peak
181 (i.e., persistent El Niño). The probability of outbreaks may reach as high as 25% along the
182 Mississippi river and over New York and central Florida. However, they are statistically
183 insignificant at the 90% confidence level. The overall low probability of outbreaks shown in
184 Figure 2e implies that the outbreak frequency is largely suppressed by a strong El Niño that

185 persists throughout the boreal spring (+1), as suggested by *Allen et al.* [2015]. However, the
186 statistical significance of the reduction cannot be established since the frequency distribution of
187 the outbreak chance is highly skewed to the right.

188 Similar to the persistent El Niño case, when a weak El Niño terminates early and cold SSTAs
189 develop over the EP in the spring (+1) (i.e., early-terminating El Niño), the probability of
190 outbreaks is also low overall (5% or less) although it increases somewhat in limited regions over
191 Missouri and northern Texas in April (+1) (Figures 2b and 2f), and over Iowa, Wisconsin and
192 Illinois in May (+1) (Figure S4f).

193 When a La Niña persists into the spring (+1) and evolves to another La Niña (i.e., resurgent
194 La Niña), the probability of outbreaks increases significantly up to 27% in April (+1) in wide
195 regions in the Ohio Valley, Southeast, Upper Midwest and Great Plains (see Figure S2 for the
196 U.S. climate regions as defined by the National Climate Data Center), particularly Nebraska,
197 Illinois, Indiana, Kentucky, Tennessee, Mississippi, Alabama, Georgia, Virginia, North Carolina
198 and Wisconsin (Figures 2c and 2g). It is interesting to note that the record-breaking 2011 tornado
199 outbreaks occurred during a resurgent La Niña. Similarly, the super tornado outbreaks in 1974
200 occurred during a resurgent La Niña.

201 As shown in Figure 2d, when a two-year La Niña transitions to an El Niño (i.e., transitioning
202 La Niña), the cold SSTAs in the CP are nearly dissipated away while the warm SSTAs in EP
203 become strong and statistically significant in MAM (+1). In this case, the probability of tornado
204 outbreaks increases strongly and significantly up to 38% in the South U.S., particularly over
205 Kansas, eastern Colorado and Texas in April (+1) (Figure 2h), and over southern Texas in March
206 (+1) (Figure S6f).

207 Two important questions arise among others as to why the probability of U.S. regional
208 tornado outbreaks increases in the spring following the peak of La Niña, and why the regions
209 affected during the resurgent La Niña case are quite different from the regions affected during
210 the transitioning La Niña case. We attempt to address these questions in the next section.

211

212 **4. Springtime Atmospheric Variability over the U.S. Linked to ENSO Phases**

213 It is well known that La Niña causes the winter atmospheric jet stream to take an unusually
214 wavy southeastward path into the U.S. from southwestern Canada, thus bringing colder and drier
215 upper level air to the U.S. Hence, the winter storm activity over the U.S. tends to increase,
216 causing more frequent wet conditions particularly over the Ohio Valley [e.g., *Ropelewski and*
217 *Halpert, 1986; Eichler and Higgins, 2006; Mo, 2010*]. As shown in Figure 3a, in the spring (+1)
218 of the resurgent La Niña case, an anomalous cyclone develops over the U.S. bringing colder and
219 drier upper-level air to the U.S., and thus the extratropical storm activity increases, suggesting
220 that the mechanism through which La Niña affects U.S. weather in winter months still prevails in
221 the spring (+1) of the resurgent La Niña case [*Lee et al., 2014a*]. The anomalous cyclone and the
222 associated increase in equivalent barotropic winds in turn enhance the low-level vertical wind
223 shear (850 - 1000 hPa) east of the Rockies, and shift the moisture stream originating from the
224 Gulf of Mexico more toward the east (Figure 3b), thus producing a set of favorable atmospheric
225 environments for tornado outbreaks in the Southeast and Ohio Valley, consistent with Figure 2g.

226 In the spring (+1) of the transitioning La Niña case, on the other hand, the extratropical storm
227 activity decreases slightly over the South and Southeast. Consistent with this feature, an
228 anomalous anticyclone forms east of the Rockies inducing anomalous southerly winds over the
229 South (Figure 3c). Therefore, the low-level vertical wind shear increases over the South and the

230 moisture stream from the Gulf of Mexico is enhanced more toward the South (Figure 3d). These
231 changes in the atmospheric environments are largely consistent with the increased probability of
232 tornado outbreaks in the South (Figure 2h).

233 The large-scale atmospheric patterns in the spring (+1) following the peak of El Niño are
234 largely opposite to those following the peak of La Niña [e.g., *Lee et al.*, 2014a]. Thus, as shown
235 in Figure S7, the atmospheric environments over the U.S. linked to the persistent and early-
236 terminating El Niño cases are largely unfavorable for tornado outbreaks, in line with Figures 2e
237 and 2f.

238

239 **5. North Atlantic SST Tripole and U.S. Regional Tornado Outbreaks**

240 As shown in Figure S8, there is a coherent and statistically significant pattern of springtime
241 SSTAs in the North Atlantic linked to the extreme U.S. tornado outbreaks (see Tables S3 for the
242 list of extreme U.S. tornado outbreak years used). This pattern is very similar to the North
243 Atlantic SST tripole, which is the dominant mode of interannual SST variability in the Atlantic
244 in boreal winter and spring and is known to be linked to multiple forcing mechanisms including
245 the North Atlantic Oscillation, tropical Atlantic variability and extratropical teleconnections from
246 the tropical Pacific [e.g., *Xie and Tanimoto*, 1998; *Okumura et al.*, 2001; *Peng et al.*, 2002; *Wu et*
247 *al.*, 2007; *Schneider and Fan*, 2012]. Hence, we further explore the potential link between the
248 North Atlantic SST tripole and the probability of U.S. regional tornado outbreaks. First, we
249 performed an empirical orthogonal function (EOF) analysis of the North Atlantic SSTAs in
250 MAM to sort the past 66 years (i.e., 1949-2014) based on the amplitude of the North Atlantic
251 SST tripole mode (i.e., the leading EOF mode). Then, we selected the top (i.e., positive) 10 cases

252 and the bottom (i.e., negative) 10 cases from the sorted years to perform composite analysis (see
253 Table S4 for the list of the positive and negative North Atlantic SST tripole years used).

254 As summarized in Figures 4 and S9, the North Atlantic SST tripole is indeed linked to the
255 probability of U.S. regional tornado outbreaks in March and April. During its negative phase
256 (i.e., cold in the tropical North Atlantic, warm in the subtropical North Atlantic and cold in the
257 subpolar North Atlantic), a robust anomalous anticyclone straddles the subtropical North Atlantic
258 extending westward over the U.S. In March, the increase in the equivalent barotropic winds
259 along the poleward half of the anomalous anticyclone enhances the low-level vertical wind shear
260 over the Upper Midwest and Ohio Valley (Figure 4b). It appears that the moisture transport
261 increases somewhat along the gulf coast mainly toward the Southeast, which is likely due to the
262 increased SSTAs in the Gulf of Mexico (Figure 4c). These changes in the low-level vertical wind
263 shear and moisture transport are fairly consistent with the significantly increased probability of
264 tornado outbreaks in the Southeast and Upper Midwest (Figure 4a). In April, the anomalous
265 anticyclone over the U.S. retreats to the east enhancing the moisture supply and the low-level
266 vertical wind shear along the South and Great Plains (Figures S9a-S9c). These relationships are
267 almost exactly the opposite during the positive phase of the North Atlantic SST tripole (Figures
268 4d-4f and S9d-S9f).

269 Although the results summarized in Figures 4 and S9 are promising, it must be noted that a
270 negative phase of the North Atlantic SST tripole forms more frequently in the early spring
271 following the peak of La Niña (Table S3). Therefore, it is unclear whether the North Atlantic
272 SST tripole adds much to the predictability of U.S. regional tornado outbreaks. Further studies
273 using model experiments and advanced statistical methods are needed to better understand the
274 impact of North Atlantic SST variability on the probability of U.S. regional tornado outbreaks.

275

276 **6. Discussion**

277 This study illustrates the links between the leading modes of springtime ENSO variability
278 and the probability of U.S. regional tornado outbreaks. However, the leading modes of El Niño
279 and La Niña variability represent only about 35% of the total variance [Lee *et al.*, 2014b]. Thus,
280 it is important to take into account the second leading modes, which represent an additional
281 approximately 28% of the total variance [Lee *et al.*, 2014b]. The two leading modes of ENSO
282 variability and the North Atlantic SST tripole mode could be used as predictors of the monthly
283 U.S. regional tornado outbreak index, using a logistic regression analysis [Cox, 1958]. The
284 regression coefficients obtained from the logistic regression analysis could be used to estimate
285 the probability of U.S. regional tornado outbreaks given the amplitudes of the three predictors.
286 Combining this statistical tool with a dynamic seasonal forecast model, which could be used to
287 obtain the three predictors with 1-3 months lead time, it might be possible to build a seasonal
288 outlook for U.S. regional tornado outbreaks. To this end, it is quite promising that high-
289 resolution climate models are now beginning to demonstrate skill in simulating and predicting
290 seasonal variations in some of the elements critical to U.S. tornado outbreak risk [e.g.,
291 *Krishnamurthy et al.*, 2015; *Yang et al.*, 2015; *Jia et al.*, 2015].

292

293 **Acknowledgments**

294 We would like to thank James Elsner and Jeff Trapp for helpful comments and suggestions on
295 the statistical methods used in this study, and Ghassan Alaka and Hua Chen for their thoughtful
296 comments and careful reviews. This work was supported by NOAA/CPO through its MAPP
297 program NA12OAR4310083 and by the base funding of NOAA/AOML. SWD and ERSST3

298 were provided by NOAA SPC at <http://www.spc.noaa.gov/wcm> and NOAA NCDC at
299 <http://www.ncdc.noaa.gov>, respectively. NCEP-NCAR reanalysis and 20CR were provided by
300 NOAA/ESRL/PSD at <http://www.esrl.noaa.gov/psd>.

301

302 **References**

303 Allen, J. T., M. K. Tippett, and A. H. Sobel (2015), Influence of the El Niño/Southern
304 Oscillation on tornado and hail frequency in the United States. *Nature Geosci.*, 8, 278–283,
305 doi:10.1038/ngeo2385.

306 Barrett, B. S., and V. A. Gensini (2013), Variability of central United States April–May tornado
307 day likelihood by phase of the Madden-Julian Oscillation. *Geophys. Res. Lett.*, 40, 2790–
308 2795.

309 Chiang J. C. H., and D. J. Vimont (2004), Analogous Pacific and Atlantic meridional modes of
310 tropical atmosphere - ocean variability. *J. Clim.*, 17, 4143–4158.

311 Compo, G. P., et al. (2011), The twentieth century reanalysis project, *Q. J. R. Meteorol. Soc.*,
312 137, 1–28, doi:10.1002/qj.776.

313 Cox, D. R. (1958), The regression analysis of binary sequences (with discussion). *J. Roy. Stat.*
314 *Soc.*, B20, 215–242.

315 Capotondi, A., et al. (2015), Understanding ENSO diversity, *Bull. Am. Meteorol. Soc.*,
316 doi:10.1175/BAMS-D-13-00117.1.

317 DiNezio, P. N., and C. Deser (2014), Nonlinear controls on the persistence of La Niña, *J. Clim.*,
318 27, 7335–7355, doi:10.1175/JCLI-D-14-00033.1.

319 Doswell, C. A., III, and L. F. Bosart (2001), Extratropical synopticscale processes and severe
320 convection. *Severe Convective Storms, Meteor. Monogr.*, No. 50, Amer. Meteor. Soc. 27–69.

321 Eichler, T., and W. Higgins (2006), Climatology and ENSO-related variability of North
322 American extratropical cyclone activity, *J. Clim.*, *19*, 2076–2093.

323 Elsner, J. B., and H. M. Widen (2014), Predicting spring tornado activity in the central Great
324 Plains by 1 March. *Mon. Weather Rev.*, *142*, 259-267.

325 Jia, L. et al., (2015), Improved seasonal prediction of temperature and precipitation over land in a
326 high-resolution GFDL climate model. *J. Clim.*, *28*, 2044-2062, doi:10.1175/JCLI-D-14-
327 00112.1.

328 Kalnay, E. et al. (1996), The NCEP/NCAR 40-year reanalysis project. *Bull. Amer. Meteor. Soc.*,
329 *77*, 437–471.

330 Krishnamurthy, L., G. Vecchi, R. Msadek, A. Wittenberg, T. Delworth, and F. Zeng, (2015), The
331 seasonality of the Great Plains low-level jet and ENSO relationship. *J. Clim.*, *28*, 4525-4544,
332 doi:10.1175/JCLI-D-14-00590.1.

333 Lee, S.-K., R. Atlas, D. B. Enfield, C. Wang and H. Liu (2013), Is there an optimal ENSO
334 pattern that enhances large-scale atmospheric processes conducive to major tornado
335 outbreaks in the U.S.? *J. Clim.*, *26*, 1626-1642, doi:10.1175/JCLI-D-12-00128.1.

336 Lee, S.-K., P. N. DiNezio, E.-S. Chung, S.-W. Yeh, A. T. Wittenberg and C. Wang (2014b)
337 Spring persistence, transition and resurgence of El Nino. *Geophys. Res. Lett.*, *41*, 8578-8585,
338 doi:10.1002/2014GL062484.

339 Lee, S.-K., B. E. Mapes, C. Wang, D. B. Enfield and S. J. Weaver (2014a), Springtime ENSO
340 phase evolution and its relation to rainfall in the continental U.S. *Geophys. Res. Lett.*, *41*,
341 1673-1680, doi:10.1002/2013GL059137.

342 Mo, K. C. (2010), Interdecadal modulation of the impact of ENSO on precipitation and
343 temperature over the United States, *J. Clim.*, *23*, 3639–3656.

344 Muñoz, E., and D. B. Enfield (2011), The boreal spring variability of the Intra-Americas low-
345 level jet and its relation with precipitation and tornadoes in the eastern United States. *Clim.*
346 *Dyn.*, 36, 247–259, doi:10.1007/s00382-009-0688-3.

347 Okumura, Y., S. P. Xie, A. Numaguti, and Y. Tanimoto (2001), Tropical Atlantic air–sea
348 interaction and its influence on the NAO. *Geophys. Res. Lett.*, 28, 1507–1510.

349 Peng, S., W. A. Robinson and S. Li (2002), North Atlantic SST forcing of the NAO and
350 relationships with intrinsic hemispheric variability, *Geophys. Res. Lett.*, 29,
351 doi:10.1029/2001GL014043, 2002.

352 Ropelewski, C. F., and M. S. Halpert (1986), North American precipitation and temperature
353 patterns associated with the El Niño - Southern Oscillation (ENSO), *Mon. Weather Rev.*, 114,
354 2352–2362.

355 Schneider, E. K. and M. Fan (2012), Observed decadal North Atlantic tripole SST variability.
356 Part II: diagnosis of mechanisms. *J. Atmos. Sci.*, 69, 51–64.

357 Smith, T. M., R. W. Reynolds, T. C. Peterson, and J. Lawrimore (2008), Improvements to
358 NOAA’s historical merged land-ocean surface temperature analysis (1880–2006), *J. Clim.*,
359 21, 2283–2296.

360 Thompson, D. B., and P. E. Roundy (2013), The relationship between the Madden-Julian
361 Oscillation and US violent tornado outbreaks in the spring. *Mon. Weather Rev.*, 141, 2087-
362 2095.

363 Tippett, M. K., A. H. Sobel, and S. J. Camargo (2012), Association of U.S. tornado occurrence
364 with monthly environmental parameters. *Geophys. Res. Lett.*, 39, L02801,
365 doi:10.1029/2011GL050368.

366 Tippett, M. K., J. T. Allen, V. A. Gensini, and H. E. Brooks (2014), Climate and hazardous
367 convective weather. *Curr. Clim. Change Rep.*, *1*, 60-73, doi:10.1007/s40641-015-0006-6.

368 Trenberth, K. E., and D. P. Stepaniak (2001), Indices of El Niño evolution. *J. Clim.*, *14*, 1697–
369 1701.

370 Verbout, S. M., H. E. Brooks, L. M. Leslie, and D. M. Schultz (2006), Evolution of the U.S.
371 tornado database: 1954–2003. *Wea. Forecasting*, *21*, 86–93.

372 Weaver, S. J., S. Baxter, and A. Kumar (2012), Climatic role of North American low-level jets
373 on U.S. regional tornado activity. *J. Clim.*, *25*, 6666 - 6683.

374 Wu, L., F. He, Z. Liu, and C. Li (2007), Atmospheric teleconnections of tropical Atlantic
375 variability: interhemispheric, tropical–extratropical, and cross-basin interactions. *J. Clim.*, *20*,
376 856–870, doi:http://dx.doi.org/10.1175/JCLI4019.1.

377 Xie, S.-P. and Y. Tanimoto (1998), A pan-Atlantic decadal climate oscillation. *Geophys. Res.*
378 *Lett.*, *25*, 2185-2155, doi:10.1029/98GL01525.

379 Yang, X. et al. (2015), Seasonal predictability of extratropical storm tracks in GFDL’s high-
380 resolution climate prediction model. *J. Clim.*, *28*, 3592-3611, doi:10.1175/JCLI-D-14-
381 00517.1.

382 Yeh, S.-W., J.-S. Kug, and S.-I. An (2014), Recent progress on two types of El Niño:
383 Observations, dynamics, and future changes, Asia-Pac. *J. Atmos. Sci.*, *50*, 69–81.

384 Yu, J.-Y., and S. T. Kim (2010), Three evolution patterns of Central-Pacific El Niño, *Geophys.*
385 *Res. Lett.*, *37*, L08706, doi:10.1029/2010GL042810.

386

387 **Figure captions:**

388 **Figure 1.** Time-longitude plots of the leading orthogonal modes of the tropical Pacific SSTAs
389 averaged between 5°S and 5°N for 21 El Niño and 22 La Niña events during 1949-2013,
390 reproduced from *Lee et al.* [2014b], namely (a) the persistent El Niño, (b) early-terminating El
391 Niño, (c) resurgent La Niña and (d) transitioning La Niña. The unit is in °C.

392

393 **Figure 2.** Composite (a-d) SSTAs for the four dominant phases of springtime ENSO evolution in
394 MAM (+1) and (e-h) the corresponding probability of U.S. regional tornado outbreaks in April
395 (+1). The gray dots in panels a-d indicate that the SSTAs are statistically significant at 90%
396 based on a student-*t* test. The black dots in panels e-h indicate that the probability of tornado
397 outbreaks is statistically significant at 90% based on a binomial test. The unit is in °C for the
398 SSTAs and in % for the probability of tornado outbreaks.

399

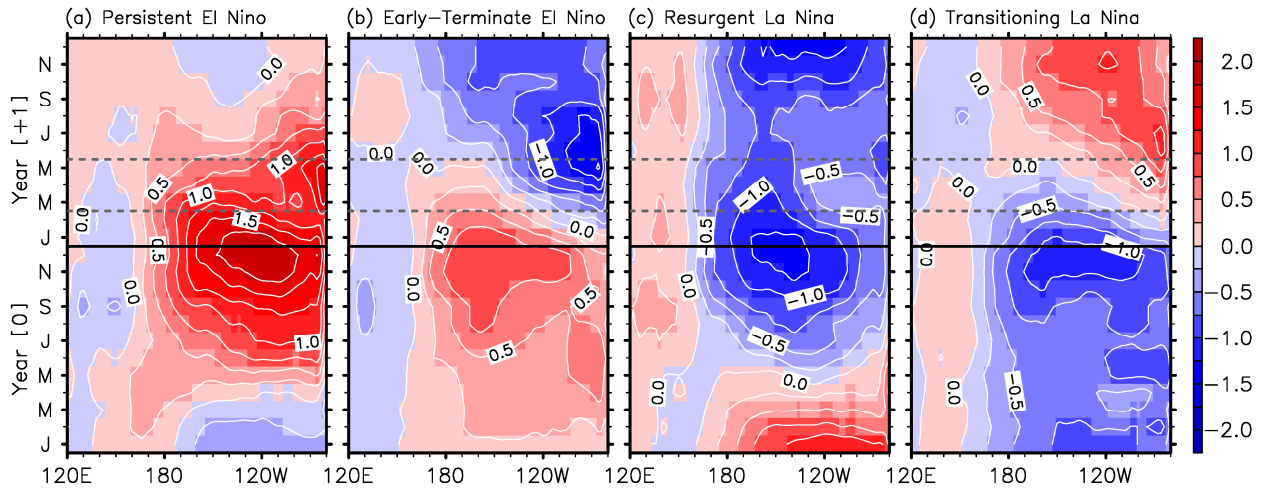
400 **Figure 3.** (upper row) Anomalous geopotential height at 500 hPa (color shades) and variance of
401 5day high-pass filtered meridional winds at 300 hPa (contours), and (lower row) anomalous
402 moisture transport (vectors) and low-level vertical wind shear (850 - 1000 hPa; color shades) in
403 MAM (+1) for (a,b) the resurgent La Niña and (c,d) transitioning La Niña cases. The units are in
404 gpm for geopotential height, in $m^2 s^{-2}$ for variance of meridional winds, in $kg m^{-1} s^{-1}$ for moisture
405 transport, and in $m s^{-1}$ for vertical wind shear.

406

407 **Figure 4.** (top row) Probability of U.S. regional tornado, (middle row) composite SSTAs (color
408 shades) and geopotential height anomalies at 500 hPa (contours), and (bottom row) low-level
409 vertical wind shear anomalies (color shades) and moisture transport anomalies (vectors) in

410 March for (a-c) the negative and (d-f) positive North Atlantic SST tripole. The unit is in % for
411 the probability of tornado outbreaks, in °C for the SSTAs, in gpm for geopotential height, in kg
412 $\text{m}^{-1} \text{s}^{-1}$ for moisture transport, and in m s^{-1} for vertical wind shear.

Leading Modes of Interevent ENSO Variability



1

2

3

4

5

6

7

8

9

10

11

12

13

14

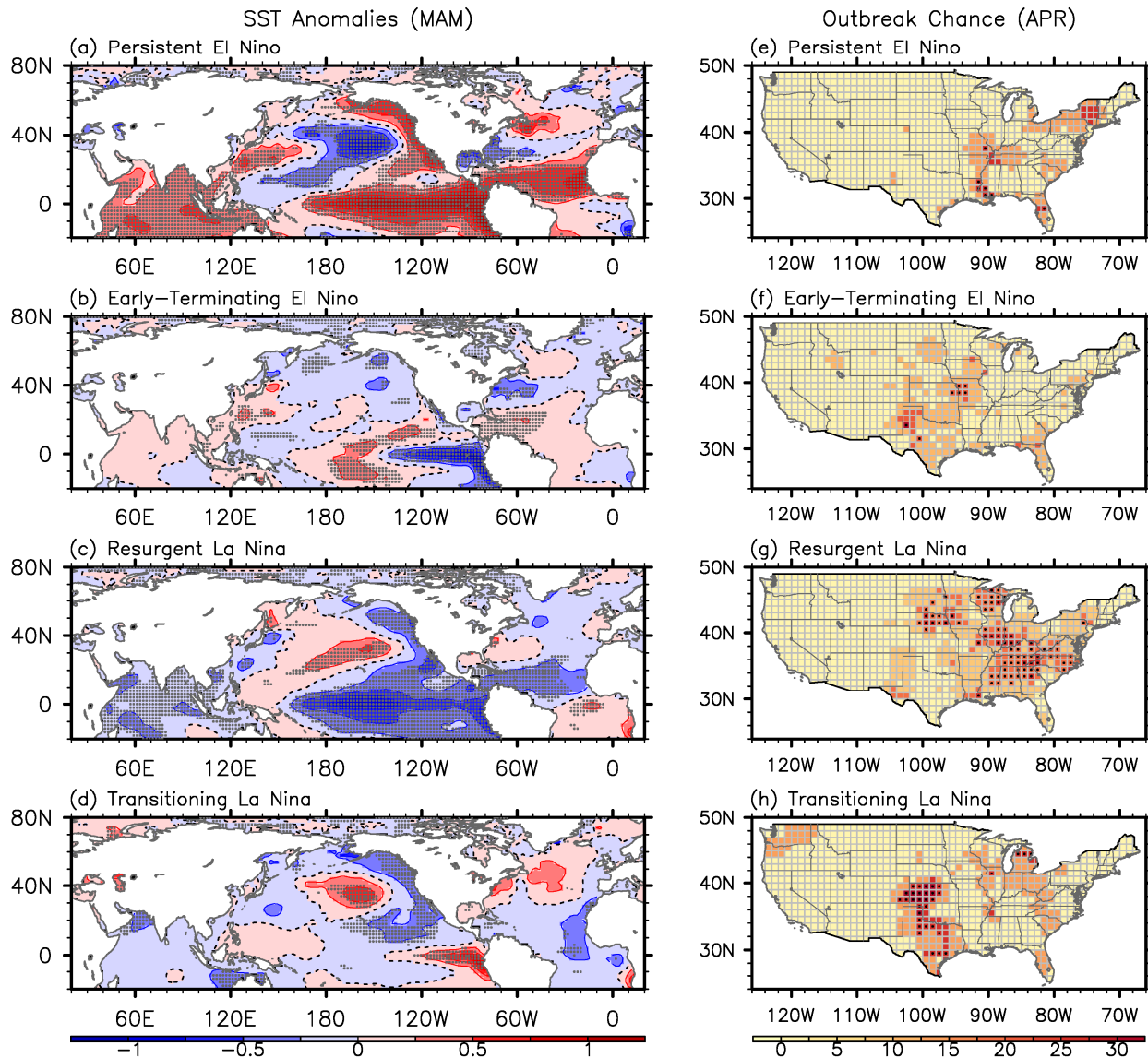
15

16

17

Figure 1. Time-longitude plots of the leading orthogonal modes of the tropical Pacific SSTAs averaged between 5°S and 5°N for 21 El Niño and 22 La Niña events during 1949-2013, reproduced from *Lee et al.* [2014b], namely (a) the persistent El Niño, (b) early-terminating El Niño, (c) resurgent La Niña and (d) transitioning La Niña. The unit is in °C.

ENSO [+1] Year: SSTA and Probability of Tornado Outbreak



18

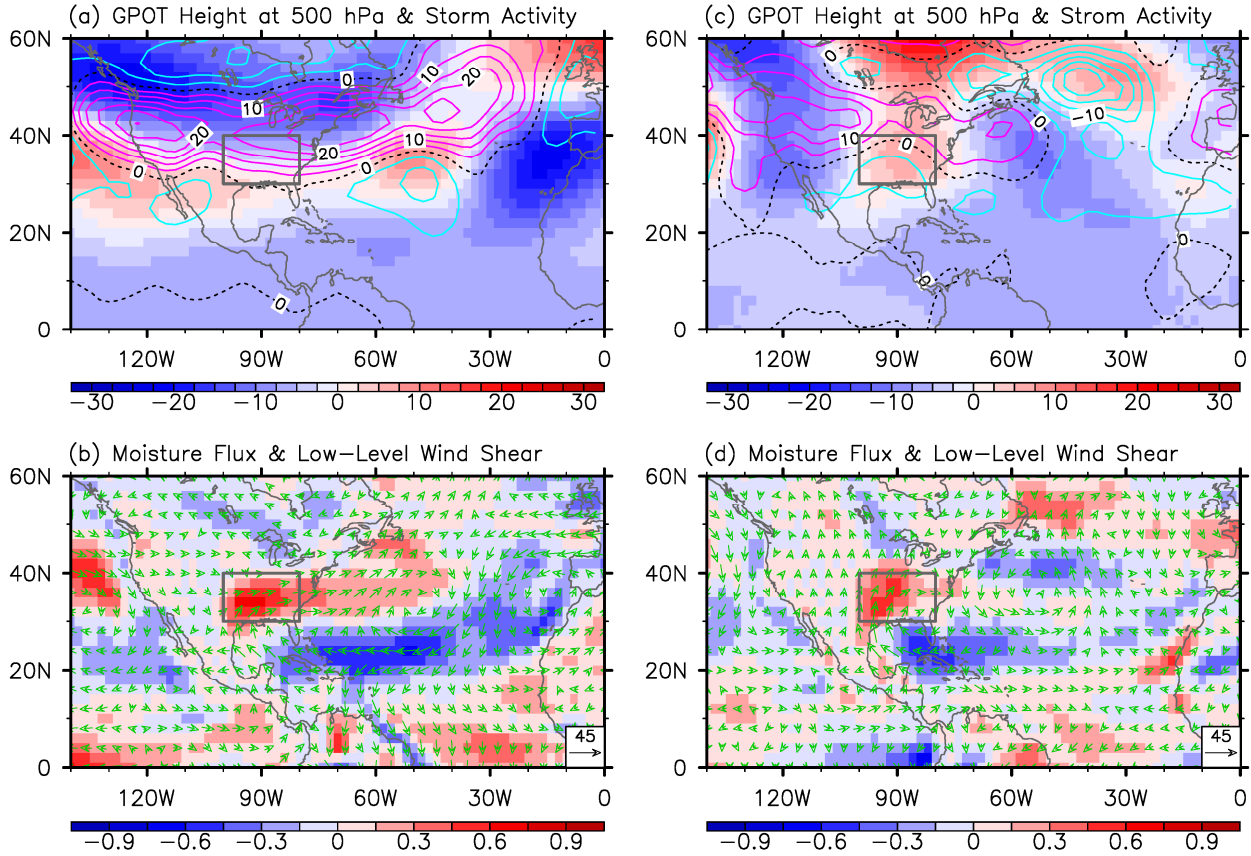
19 **Figure 2.** Composite (a-d) SSTAs for the four dominant phases of springtime ENSO evolution in
 20 MAM (+1) and (e-h) the corresponding probability of U.S. regional tornado outbreaks in April
 21 (+1). The gray dots in panels a-d indicate that the SSTAs are statistically significant at 90%
 22 based on a student-*t* test. The black dots in panels e-h indicate that the probability of tornado
 23 outbreaks is statistically significant at 90% based on a binomial test. The unit is in °C for the
 24 SSTAs and in % for the probability of tornado outbreaks.

25

La Nina [+1] Year (MAM): Atmospheric Anomalies over the U.S.

Resurgent La Nina

Transitioning La Nina



26

27

28

29

30

31

32

33

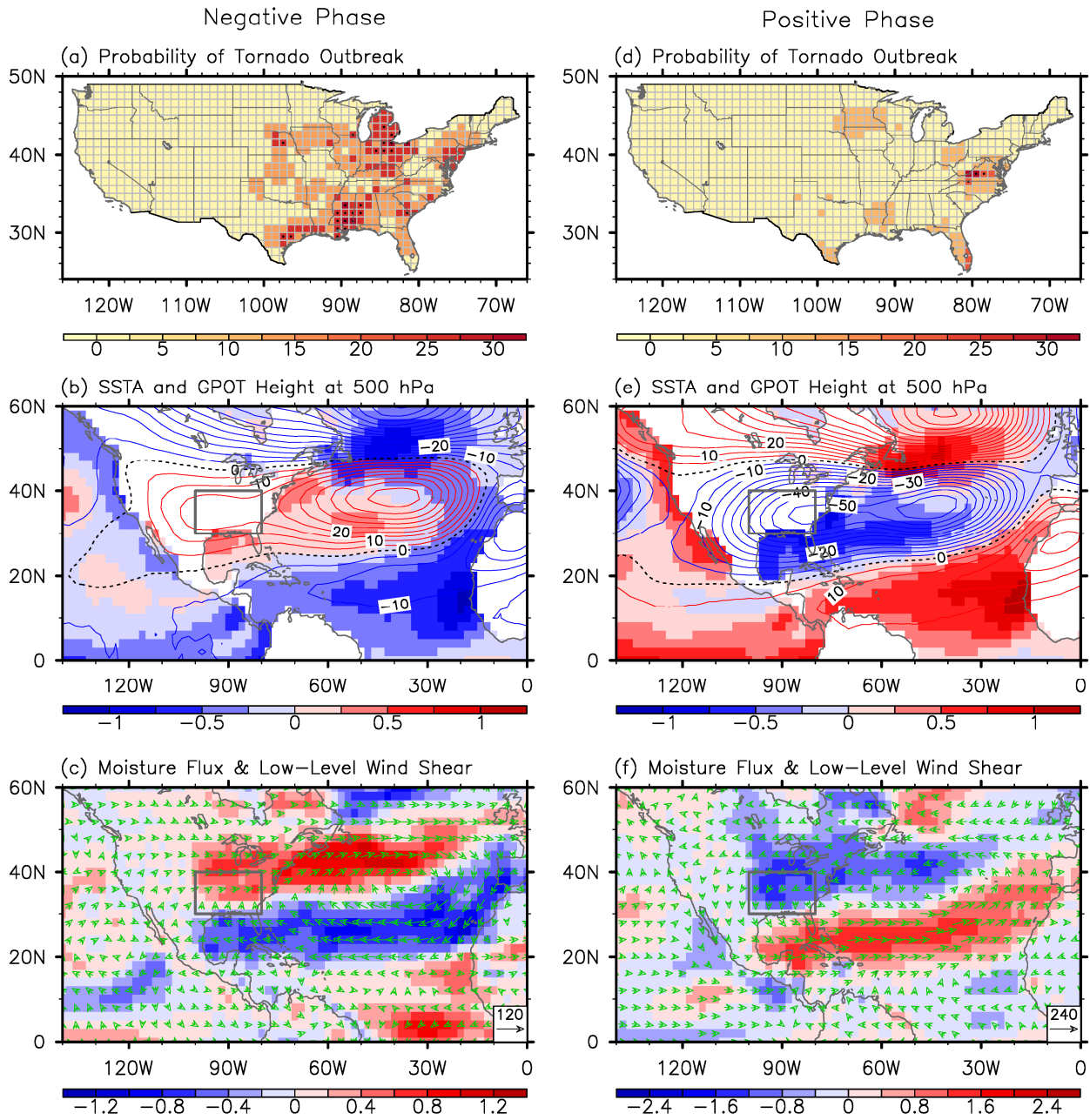
34

35

36

Figure 3. (upper row) Anomalous geopotential height at 500 hPa (color shades) and variance of 5day high-pass filtered meridional winds at 300 hPa (contours), and (lower row) anomalous moisture transport (vectors) and low-level vertical wind shear (850 - 1000 hPa; color shades) in MAM (+1) for (a,b) the resurgent La Niña and (c,d) transitioning La Niña cases. The units are in gpm for geopotential height, in $m^2 s^{-2}$ for variance of meridional winds, in $kg m^{-1} s^{-1}$ for moisture transport, and in $m s^{-1}$ for vertical wind shear.

NATL Tripole Mode (MAR): Outbreak Chance, SSTA & Atmospheric Anomalies



37

38 **Figure 4.** (top row) Probability of U.S. regional tornado, (middle row) composite SSTAs (color
 39 shades) and geopotential height anomalies at 500 hPa (contours), and (bottom row) low-level
 40 vertical wind shear anomalies (color shades) and moisture transport anomalies (vectors) in
 41 March for (a-c) the negative and (d-f) positive North Atlantic SST tripole. The unit is in % for

- 42 the probability of tornado outbreaks, in °C for the SSTAs, in gpm for geopotential height, in kg
- 43 $\text{m}^{-1} \text{s}^{-1}$ for moisture transport, and in m s^{-1} for vertical wind shear.

1 **Table S1.** Tornado-related number of fatalities and injuries and property and crop damages (in
 2 million US dollars) in the U.S. during 2004-2013, reproduced from the U.S. Natural Hazard
 3 Statistics (<http://www.nws.noaa.gov/om/hazstats.shtml>).

Year	Fatalities	Injuries	Property & crop damages
2004	35	396	549.2
2005	38	537	503.9
2006	64	990	759.0
2007	81	659	1,407.5
2008	126	1,714	1,865.6
2009	21	351	584.9
2010	45	699	1,134.6
2011	553	5,483	9,493.0
2012	70	822	1,649.7
2013	55	756	3,648.7
Total	1,091	12,407	21,596.1

4
 5
 6
 7
 8
 9
 10
 11
 12
 13
 14
 15
 16
 17
 18

19 **Table S2.** List of four leading cases of ENSO variability (i.e., 8 persistent El Niño, 10 early-
 20 terminating El Niño, 11 resurgent La Niña and 8 transitioning La Niña cases) identified based on
 21 the sign and amplitude of the principal components of interevent El Niño and La Niña variability
 22 during 1949 - 2013 [Lee *et al.*, 2014b]. These ENSO events are listed by their onset-decay years
 23 (i.e., year (0) - year (+1)). Note that the four leading cases of ENSO variability describe ENSO
 24 phase evolution in the spring (+1) following the peak of ENSO in boreal winter.

Persistent El Niño	Early-Terminating El Niño	Resurgent La Niña	Transitioning La Niña
1957 - 1958	1951 - 1952	1949 - 1950	1950 - 1951
1968 - 1969	1953 - 1954	1955 - 1954	1956 - 1957
1982 - 1983	1963 - 1964	1970 - 1971	1964 - 1965
1986 - 1987	1965 - 1966	1973 - 1974	1971 - 1972
1991 - 1992	1969 - 1970	1974 - 1975	1975 - 1976
1997 - 1998	1972 - 1973	1983 - 1984	2000 - 2001
2004 - 2005	1977 - 1978	1984 - 1985	2005 - 2006
2009 - 2010	1987 - 1988	1988 - 1989	2011 - 2012
	1994 - 1995	1995 - 1996	
	2006 - 2007	1998 - 1999	
		2010 - 2011	

25
 26
 27
 28
 29
 30
 31
 32
 33
 34
 35
 36

37 **Table S3.** List of 10 most active and 10 least active U.S. tornado years based on the total number
 38 of F1-F5 tornados in the U.S. during MAM. The corresponding ENSO phase for each case is
 39 also shown. Note that the decaying phase of 2008 La Niña cannot be described using the leading
 40 mode of observed La Niña variability; thus it is simply referred to as decaying La Niña. The
 41 onset of El Niño in 1982 occurred from ENSO neural condition; thus it is referred to as
 42 developing El Niño as in cases of 1991 and 2002.

10 Most Active U.S. Tornado Years		10 Least Active U.S. Tornado Years	
Year (Number)	ENSO phases	Year (Number)	ENSO phases
2011 (690)	Resurgent La Niña	1951 (67)	Transition La Niña
1973 (412)	Early-Term El Niño	1987 (80)	Persistent El Niño
1974 (390)	Resurgent La Niña	1950 (89)	Resurgent La Niña
2008 (359)	Decaying La Niña	2005 (89)	Persistent El Niño
1982 (342)	Developing El Niño	1952 (93)	Early-Term El Niño
1976 (325)	Transition La Niña	1992 (102)	Persistent El Niño
1957 (317)	Transition La Niña	1958 (113)	Persistent El Niño
2003 (306)	Persistent El Niño	2002 (125)	Developing El Niño
1991 (302)	Developing El Niño	1993 (129)	ENSO neutral
1965 (301)	Transition La Niña	1969 (130)	Persistent El Niño

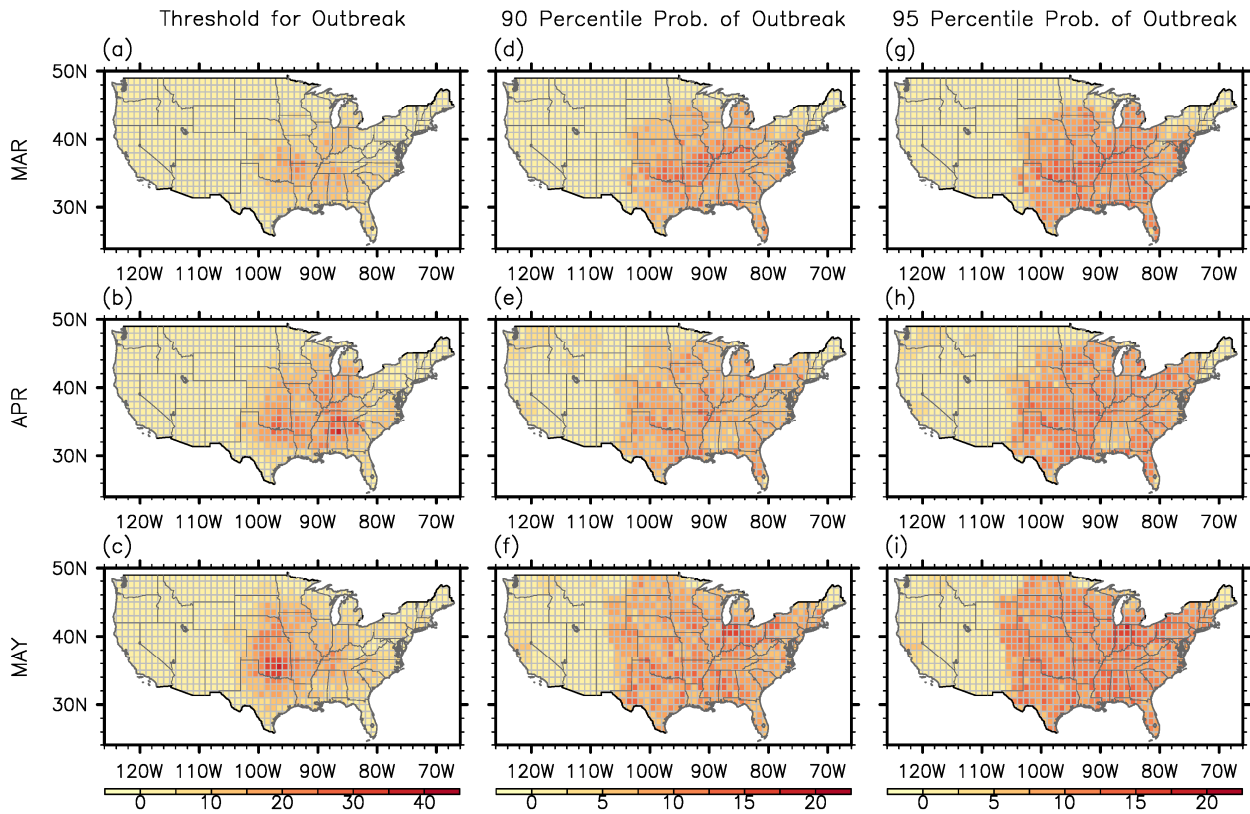
43
 44
 45
 46
 47
 48
 49
 50
 51
 52
 53
 54
 55

56 **Table S4.** List of 10 negative and 10 positive phases of North Atlantic SST tripole mode in
 57 MAM during 1949-2014, derived from the leading EOF mode of the North Atlantic SSTAs in
 58 MAM. For each case of the positive and negative phase of North Atlantic SST tripole mode, the
 59 corresponding springtime ENSO phase is also listed. Note that the onset of El Niño in 1986
 60 occurred from ENSO neural condition; thus it is referred to as developing El Niño as in cases of
 61 1991, 1994 and 2009.

Negative phase of North Atlantic SST tripole (MAM)		Positive phase of North Atlantic SST tripole (MAM)	
Year	ENSO phases	Year	ENSO phases
1972	Transition La Niña	1951	Transition La Niña
1974	Resurgent La Niña	1958	Persistent El Niño
1975	Resurgent La Niña	1966	Early-Term El Nino
1976	Transition La Niña	1969	Persistent El Niño
1985	Resurgent La Niña	1970	Early-Term El Nino
1986	Developing El Niño	1981	ENSO neutral
1989	Resurgent La Niña	1983	Persistent El Niño
1991	Developing El Niño	1998	Persistent El Niño
1994	Developing El Niño	2005	Persistent El Niño
2009	Developing El Niño	2010	Persistent El Niño

62
 63
 64
 65
 66
 67
 68
 69
 70
 71
 72
 73

Monthly Max 5-Day Running Total Weighted Number of Tornadoes within 200 km Radius



74

75 **Figure S1.** (a-c) Outbreak threshold of monthly maximum 5-day running total weighted number
76 of F1 – F5 tornadoes within the 200 km radius, (d-f) the 90 percentile probability of U.S.
77 regional outbreaks, and (g-i) the 95 percentile probability of U.S. regional tornado outbreaks for
78 (top row) March, (middle row) April and (bottom row) May. Bootstrap method is used to
79 determine the 90th and 95th percentile probabilities (%) of outbreak. See section 2 for more
80 details about how these fields are derived.

81

82

83

84

85

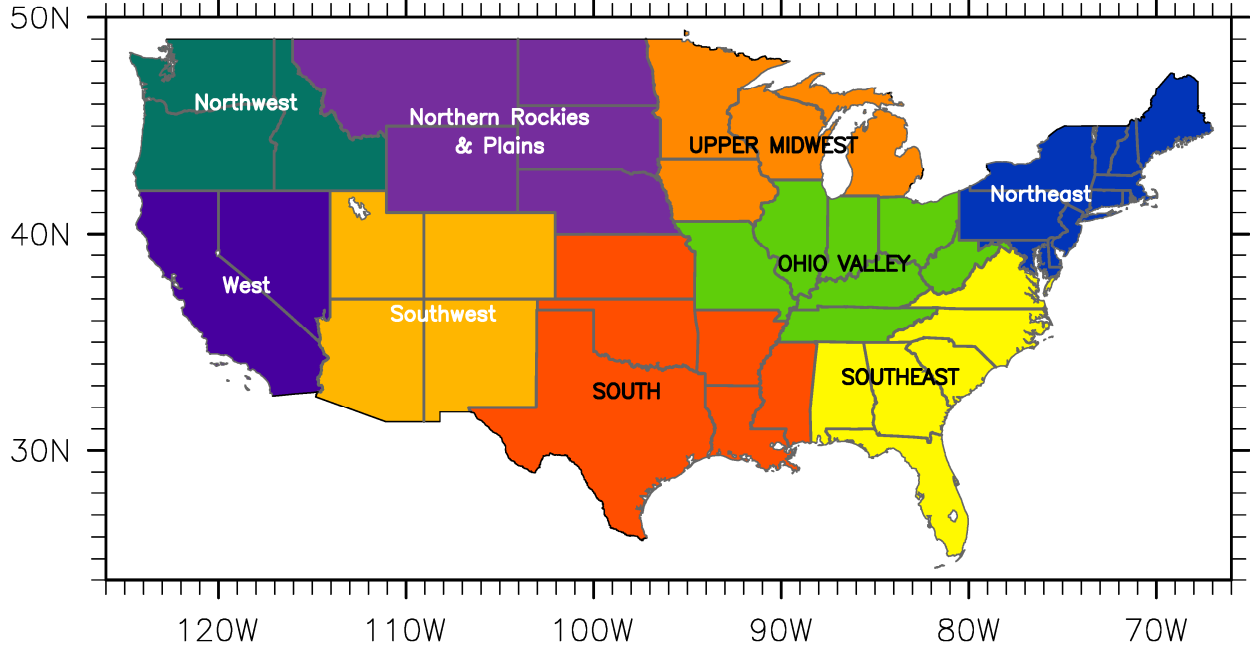
86

87

88

89

U.S. Climate Regions defined by NCDC



90

91 **Figure S2.** U.S. climate regions defined by National Climate Data Center. The four regions,
92 namely the South, Ohio Valley, Southeast and Upper Midwest, are frequently referred in the
93 main text to describe the probability of U.S. regional tornado outbreaks.

94

95

96

97

98

99

100

101

102

103

104

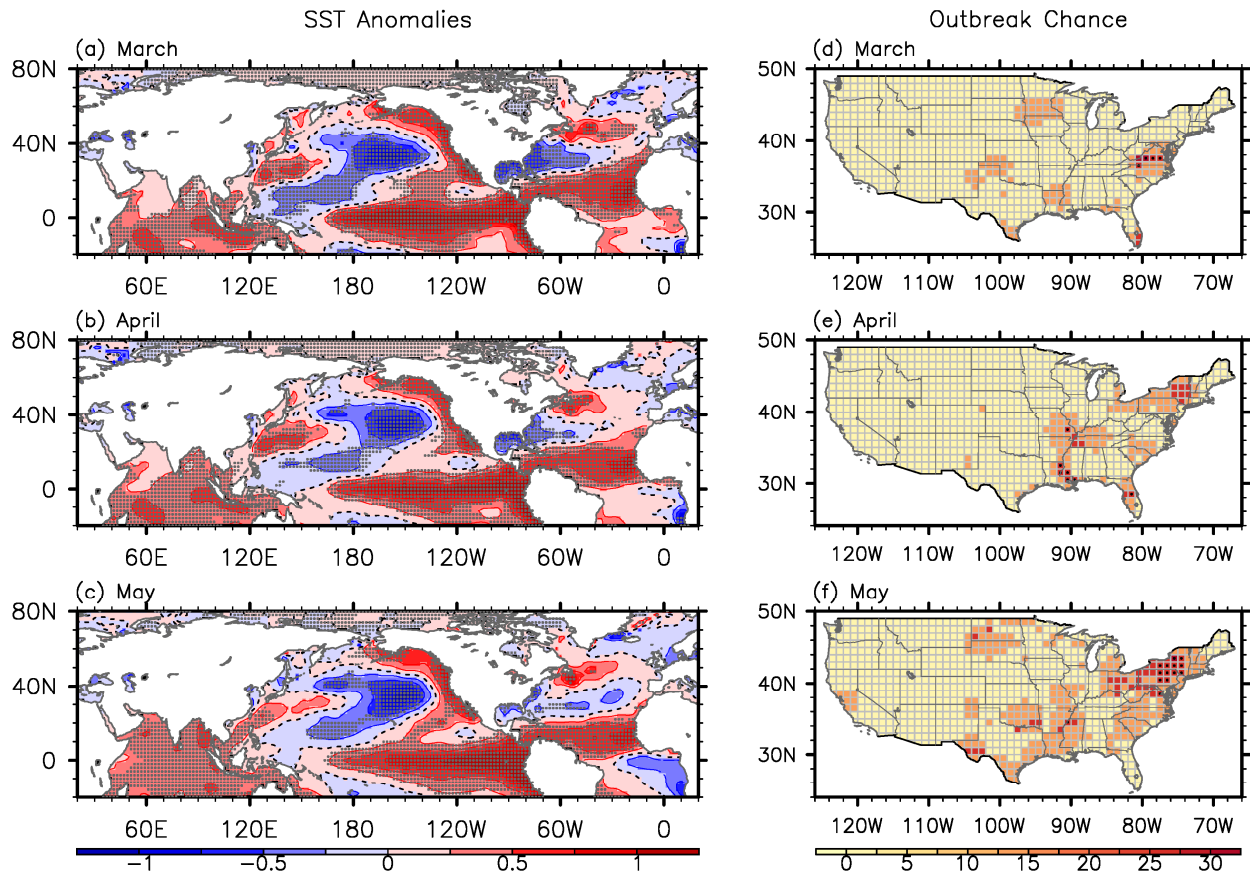
105

106

107

108

Persistent El Niño [+1] Year: SSTA and Probability of Tornado Outbreak



109

110 **Figure S3.** Composite (a-c) SSTAs for the persistent El Niño case and (d-f) the corresponding
111 probability of U.S. regional tornado outbreaks in (top row) March (+1), (middle row) April (+1)
112 and (bottom row) May (+1). The gray dots in panels a-c indicate that the SSTAs are statistically
113 significant at 90% based on a Student's *t*-test. The black dots in panels d-f indicate that the
114 probability of tornado outbreaks is statistically significant at 90% based on a binomial test. The
115 unit is in °C for the SSTAs and in % for the probability of tornado outbreaks.

116

117

118

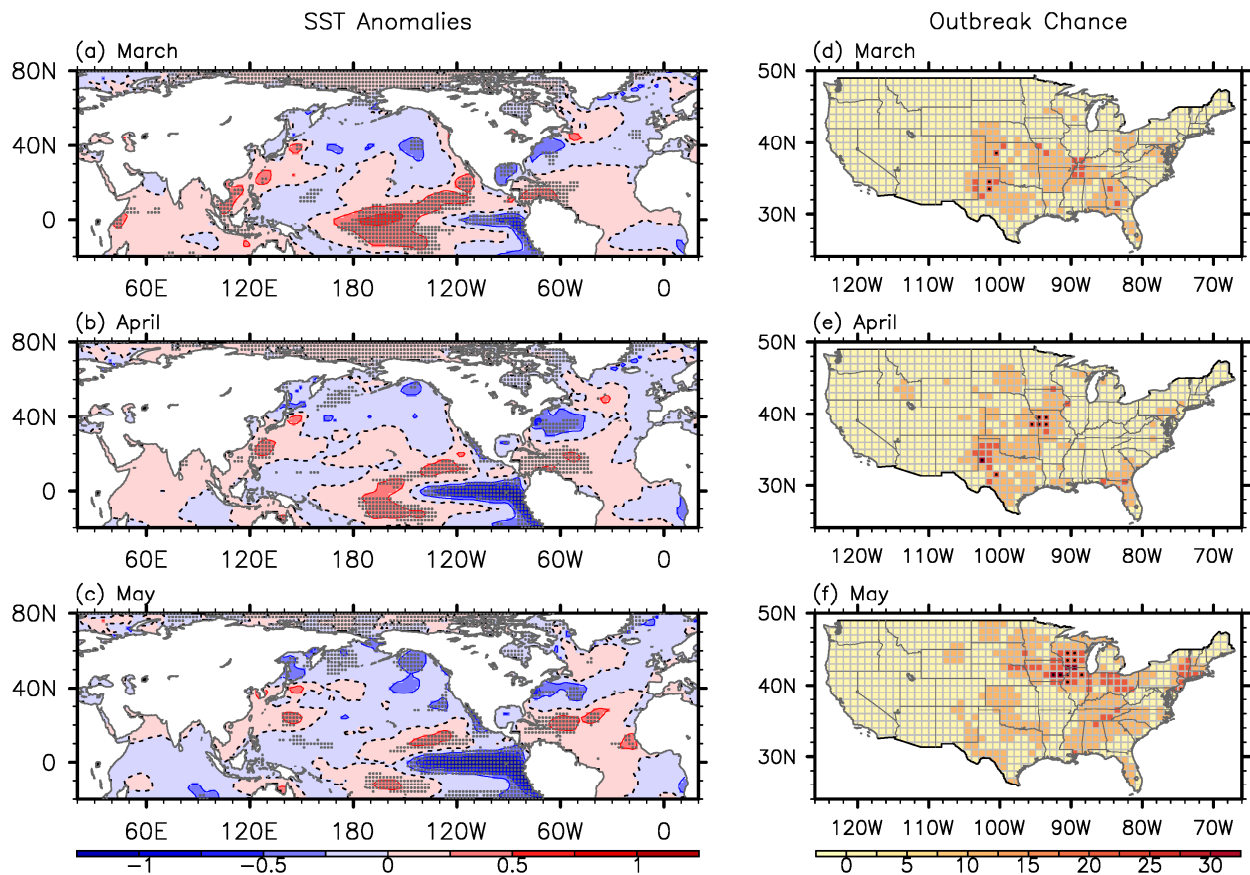
119

120

121

122

Early-Terminating El Niño [+1] Year: SSTA and Probability of Tornado Outbreak



123

124 **Figure S4.** Composite (a-c) SSTAs for the early-terminating El Niño case and (d-f) the
125 corresponding probability of U.S. regional tornado outbreaks in (top row) March (+1), (middle
126 row) April (+1) and (bottom row) May (+1). The gray dots in panels a-c indicate that the SSTAs
127 are statistically significant at 90% based on a Student's *t*-test. The black dots in panels d-f
128 indicate that the probability of tornado outbreaks is statistically significant at 90% based on a
129 binomial test. The unit is in °C for the SSTAs and in % for the probability of tornado outbreaks.

130

131

132

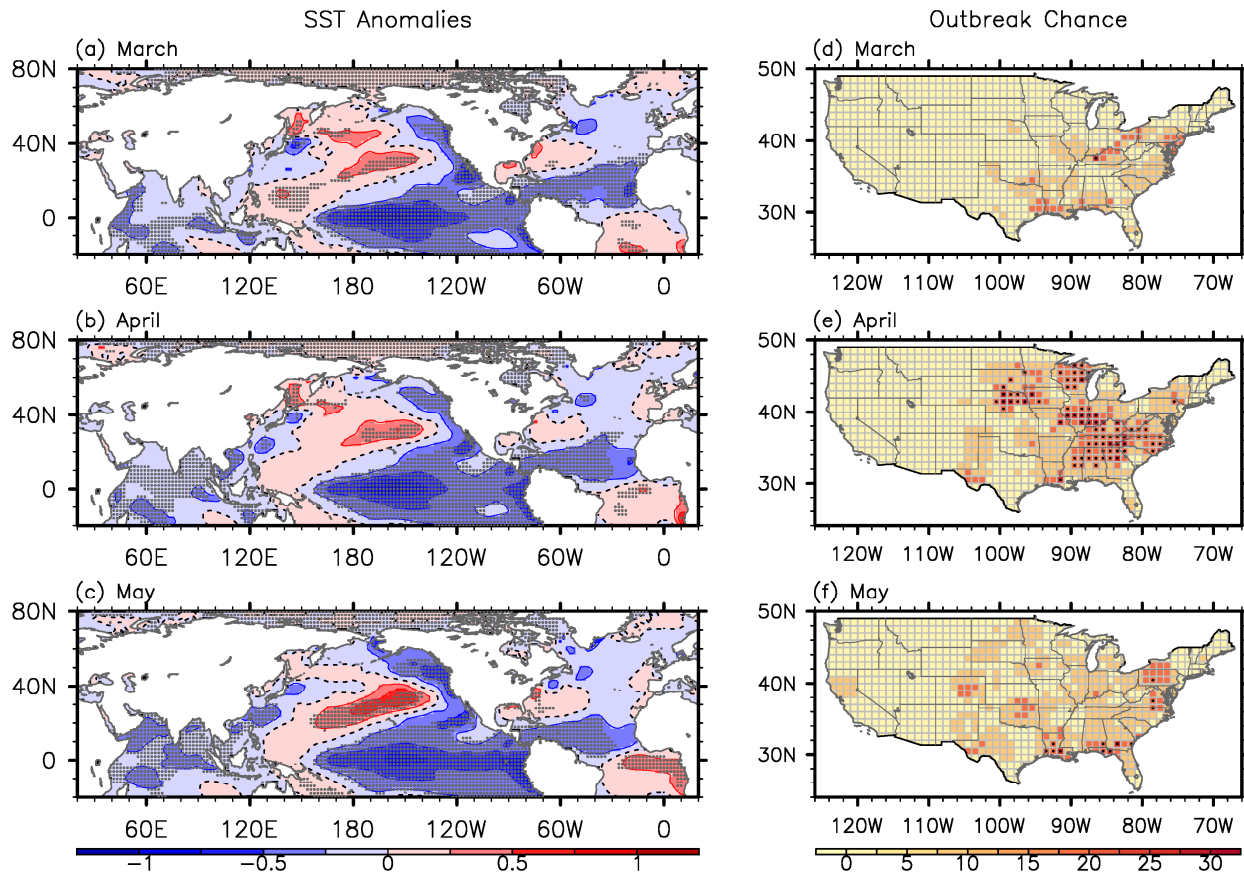
133

134

135

136

Resurgent La Nina [+1] Year: SSTA and Probability of Tornado Outbreak



137

138 **Figure S5.** Composite (a-c) SSTAs for the resurgent La Niña case and (d-f) the corresponding
139 probability of U.S. regional tornado outbreaks in (top row) March (+1), (middle row) April (+1)
140 and (bottom row) May (+1). The gray dots in panels a-c indicate that the SSTAs are statistically
141 significant at 90% based on a Student's *t*-test. The black dots in panels d-f indicate that the
142 probability of tornado outbreaks is statistically significant at 90% based on a binomial test. The
143 unit is in °C for the SSTAs and in % for the probability of tornado outbreaks.

144

145

146

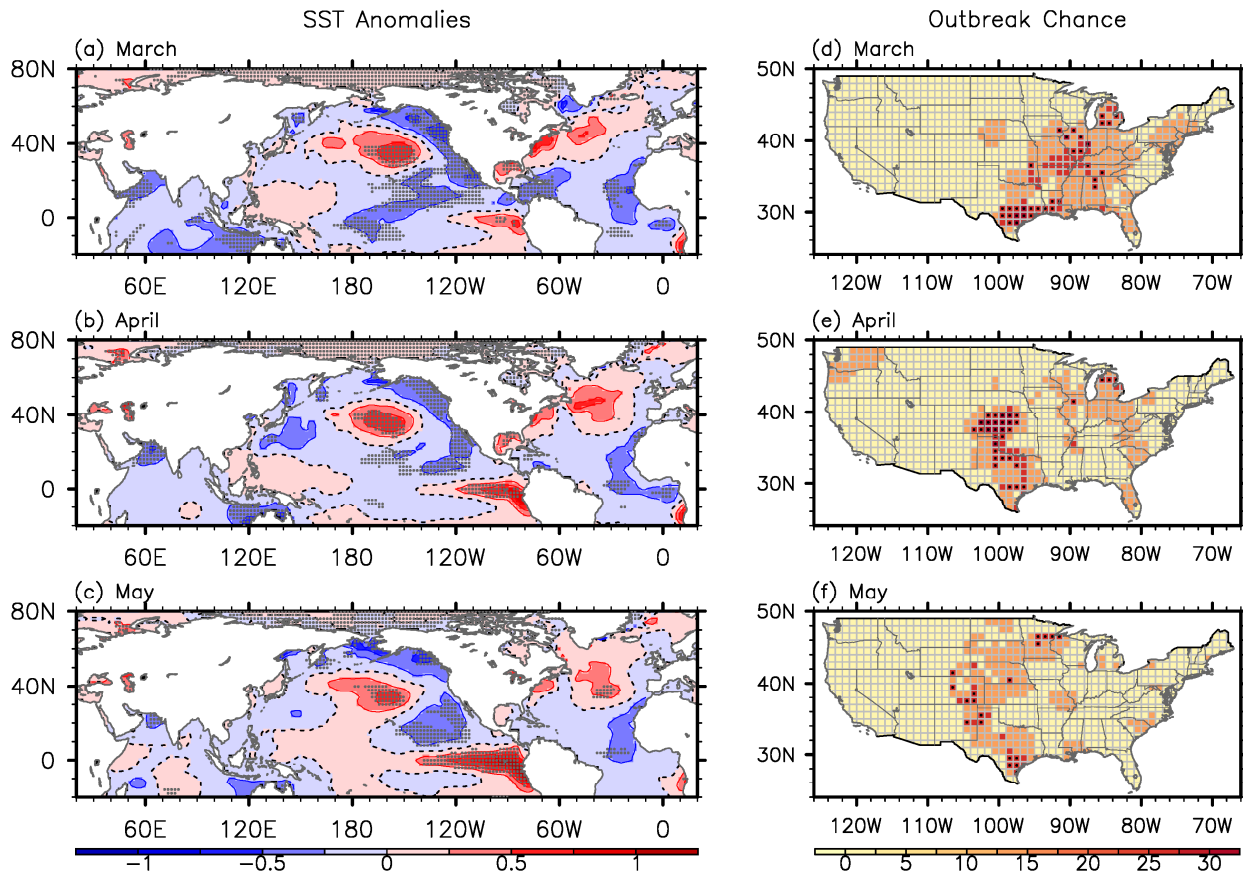
147

148

149

150

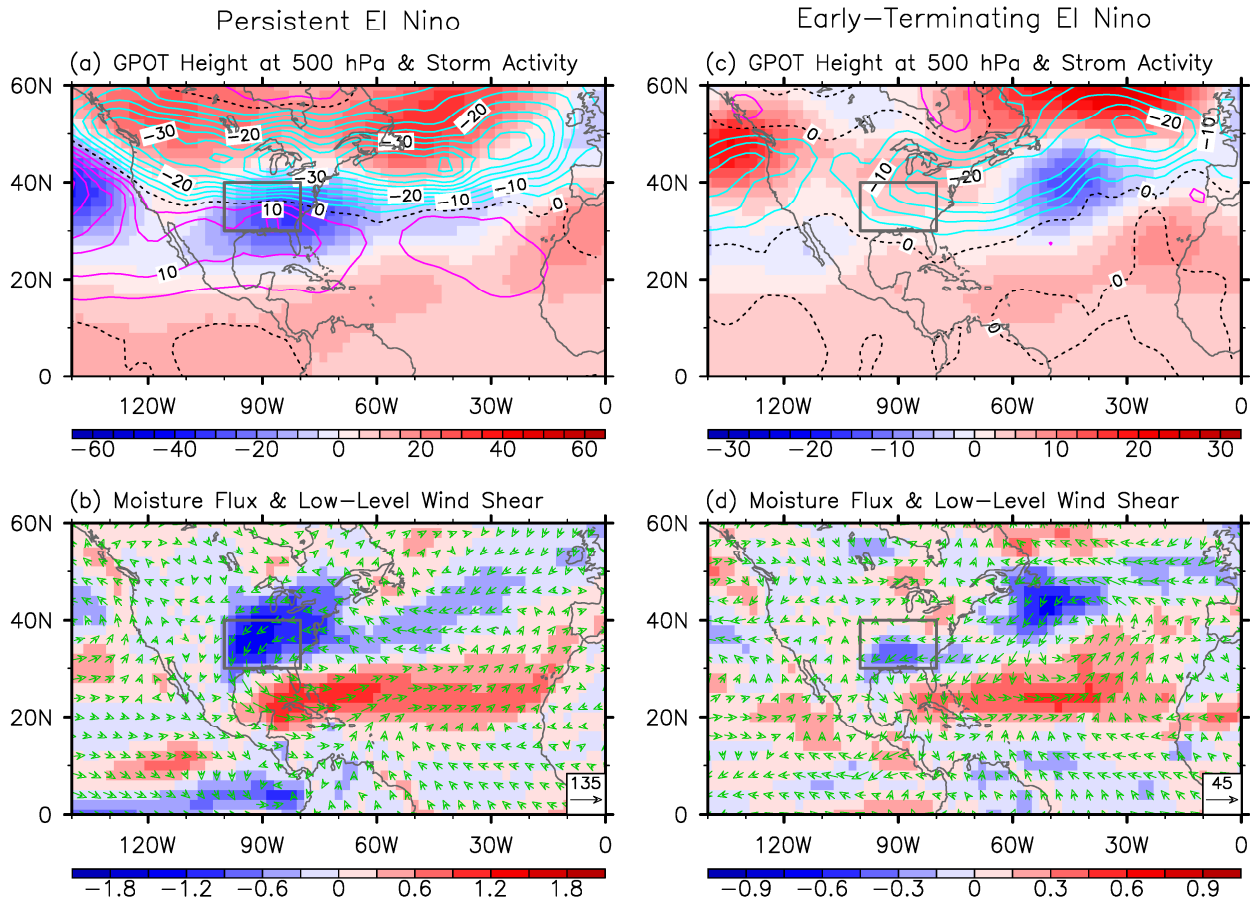
Transitioning La Nina [+1] Year: SSTA and Probability of Tornado Outbreak



151
152 **Figure S6.** Composite (a-c) SSTAs for the transitioning El Niño case and (d-f) the corresponding
153 probability of U.S. regional tornado outbreaks in (top row) March (+1), (middle row) April (+1)
154 and (bottom row) May (+1). The gray dots in panels a-c indicate that the SSTAs are statistically
155 significant at 90% based on a Student's *t*-test. The black dots in panels d-f indicate that the
156 probability of tornado outbreaks is statistically significant at 90% based on a binomial test. The
157 unit is in °C for the SSTAs and in % for the probability of tornado outbreaks.

158
159
160
161
162
163
164
165

El Niño [+1] Year (MAM): Atmospheric Anomalies over the U.S.



166

167 **Figure S7.** (upper row) Anomalous geopotential height at 500 hPa (color shades) and variance of
168 5day high-pass filtered meridional winds at 300 hPa (contours), and (lower row) anomalous
169 moisture transport (vectors) and low-level vertical wind shear (850 - 1000 hPa; color shades) in
170 MAM (+1) for (a,b) the persistent El Niño and (c,d) early-terminating El Niño cases. The units
171 are in gpm for geopotential height, in $m^2 s^{-2}$ for variance of meridional winds, in $kg m^{-1} s^{-1}$ for
172 moisture transport, and in $m s^{-1}$ for vertical wind shear.

173

174

175

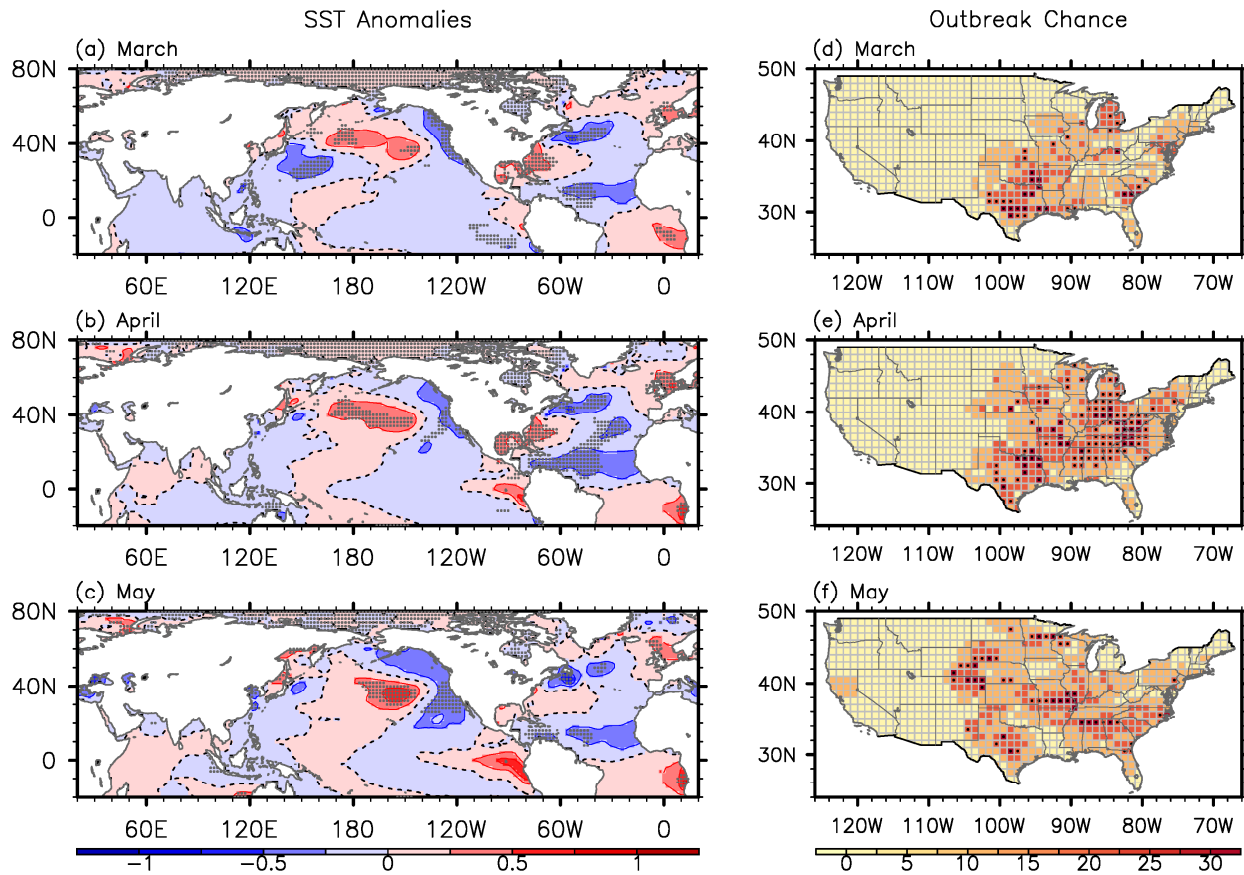
176

177

178

179

Active US Tornado Years: SSTA and Probability of Tornado Outbreak



180

181 **Figure S8.** Composite (a-c) SSTAs for the 10 most active U.S. tornado years and (d-f) the
182 corresponding probability of U.S. regional tornado outbreaks in (top row) March, (middle row)
183 April and (bottom row) May. The gray dots in panels a-c indicate that the SSTAs are statistically
184 significant at 90% based on a student-*t* test. The black dots in panels d-f indicate that the
185 probability of tornado outbreaks is statistically significant at 90% based on a Chi-square test. The
186 unit is in °C for the SSTAs and in % for the probability of tornado outbreaks.

187

188

189

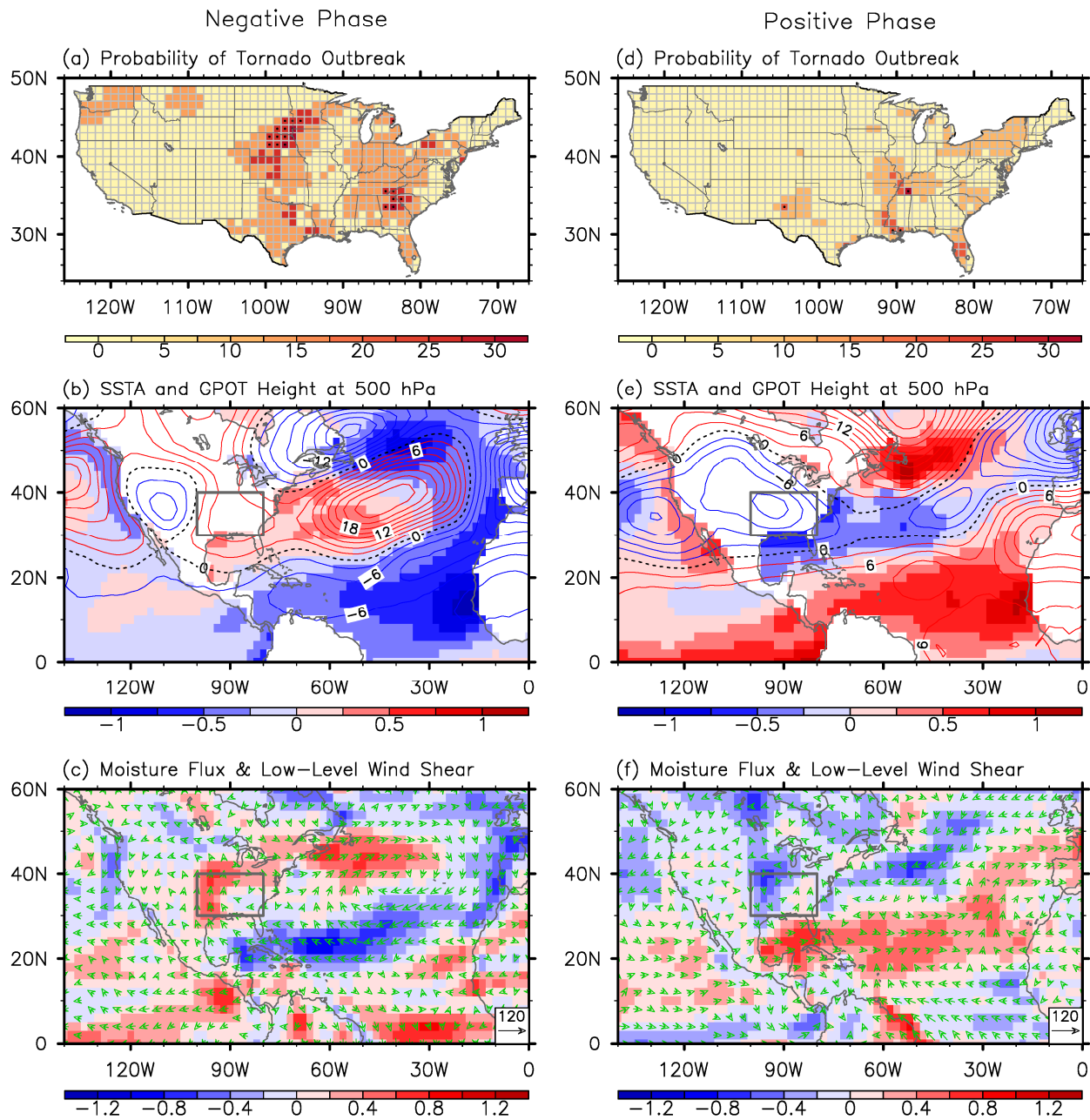
190

191

192

193

NATL Tripole Mode (APR): Outbreak Chance, SSTA & Atmospheric Anomalies



194
 195 **Figure S9.** (top row) Probability of U.S. regional tornado, (middle row) composite SSTAs (color
 196 shades) and geopotential height anomalies at 500 hPa (contours), and (bottom row) low-level
 197 vertical wind shear anomalies (color shades) and moisture transport anomalies (vectors) in April
 198 for (a-c) the negative and (d-f) positive North Atlantic SST tripole. The unit is in % for the
 199 probability of tornado outbreaks, in °C for the SSTAs, in gpm for geopotential height, in kg m⁻¹
 200 s⁻¹ for moisture transport, and in m s⁻¹ for vertical wind shear.